JOURNAL OF GUIDANCE, CONTROL, AND DYNAMICS
Vol. 30, No. 4, July–August 2007

Real-Time Nonlinear Embedded Control for an Autonomous Quadrotor Helicopter

F. Kendoul,* D. Lara,† I. Fantoni-Coichot,‡ and R. Lozano§
Université de Technologie de Compiègne, 60200 Compiègne, France

DOI: 10.2514/1.27882

Control system design of aerospace vehicles with actuator saturation is an important practical design problem that many previous approaches to nonlinear autopilot design did not consider. In particular, small unmanned aerial vehicle rotorcraft actuators often have physical limitations such as a restricted onboard power supply. Disregard of actuator saturation can affect the final performance, but the reduction in performance can be mitigated if actuator saturation is included in the controller design. In this paper, we propose a nested-saturation-based nonlinear controller for the stabilization of a rotary-wing aircraft. This control strategy allows the incorporation of actuator magnitude saturation and has satisfactory dynamic performance. The nested-saturation technique enables the controller to ensure the global asymptotic stability of a quadrotor helicopter while improving the performance of the closed-loop system. By using Lyapunov analysis, the convergence property is established for the complete nonlinear model of the quadrotor rotorcraft. Simulation results show the performance of the proposed control strategy. Using embedded sensors and onboard control, we performed a real-time autonomous flight. Indeed, experimental results have shown that the proposed control strategy is able to autonomously perform the tasks of taking off, hovering, and landing.

Nomenclature

A, D	=	horizontal-movement model matrices
a, b, c, d	=	saturation levels
$C(\dot{\eta}, \eta)$	=	Coriolis/centripetal vector
$c_{(.)}$	=	cos( )
F	=	force vector generated by propellers and expressed in $\mathcal{B}$
F^{ext}	=	generalized force vector
g	=	Earth's gravitational acceleration
$\mathcal{I}$	=	inertial reference frame
I_p	=	rotor-blade moment of inertia
$\mathbb{I}(\eta)$	=	pseudoinertia matrix
J	=	inertia matrix
k, K	=	controller scalar gains, controller gain matrices
L_θ, L_ϕ	=	limits of $\lvert\theta\rvert$ and $\lvert\phi\rvert$ when $t \to \infty$
l	=	distance from the rotors to the helicopter center of mass
M	=	upper bound of the coupling term D
m	=	aircraft mass
R	=	rotation matrix from $\mathcal{B}$ to $\mathcal{I}$
r	=	new input for altitude control
$s_{(.)}$	=	sin( )
$T_1, \ldots, T_5$	=	finite times
u	=	total main-propellers' thrust
w_i	=	angular speed of the rotor i
$\mathcal{B}$	=	body reference frame
$\eta = (\phi, \theta, \psi)$	=	Euler angles (roll, pitch, yaw)
μ, κ	=	propellers' lift and drag coefficients
$\upsilon^{\mathcal{B}}$	=	body linear velocity
$\upsilon^{\mathcal{I}}$	=	body velocity in $\mathcal{I}$
$\xi = (x, y, z)$	=	components of the position vector of the system mass center in the inertial frame
$\tilde{\xi}$, $\tilde{\eta}$	=	reduced position (x, y) and orientation (ϕ, θ) vectors
$\sigma(.)$	=	saturation function
τ	=	generalized torque vector in the body reference frame
Ω	=	body angular velocity

Subscripts

d	=	desired
i	=	variable number
0	=	initial

Received 19 September 2006; revision received 18 January 2007; accepted for publication 22 January 2007.

*Ph.D. Student, Heudiasyc Laboratory, Unite Mixte de Recherche 6599, Centre National de la Recherche Scientifique; fkendoul@hds.utc.fr.

†Ph.D. Student, Heudiasyc Laboratory, Unite Mixte de Recherche 6599, Centre National de la Recherche Scientifique; dlara@hds.utc.fr.

‡Centre National de la Recherche Scientifique Researcher, Heudiasyc Laboratory, Unite Mixte de Recherche 6599; ifantoni@hds.utc.fr.

§Centre National de la Recherche Scientifique Researcher, Heudiasyc Laboratory, Unite Mixte de Recherche 6599; rlozano@hds.utc.fr.

I. Introduction

IN THE last decade, we have witnessed significant progress toward the development of autonomous aerial vehicles with onboard intelligent capabilities. These systems open new applications in the field of robotics including surveillance, disaster (environmental, industrial, and urban) assistance, search and rescue, data and image acquisition of targets and affected areas, and many others.

Recently, new small flying robots, called organics or mini unmanned aerial vehicles (UAVs), such as Pointer, Javelin, Black Pack Mini, and other configurations have appeared [1]. Furthermore, many different vertical takeoff and landing (VTOL) UAVs, including conventional helicopters [2,3], quadrotor aircraft [4], two-tilt-rotor rotorcraft [5], and several designs such as the Guardian from Bombardier, the Sikorksy Cypher, and the DragonWarrior have been extensively studied. Aerial robotics has mainly involved helicopters and other VTOL designs, airships, and fixed-wing UAVs [6,7]. The main advantage of helicopters and other VTOL platforms is their maneuverability, necessary for many robotic applications. Indeed, the ability to maintain the aerial vehicle in hover is very important in many tasks. However, rotary-wing aircraft are difficult to control and require the application of reliable and nonlinear control laws. Indeed,

the dynamic performance of aerospace systems such as aircraft is highly dependent on the capabilities of the guidance, navigation, and control systems. To achieve improved performance in such aerospace systems, it is important that more appropriate control systems be developed and implemented.

A. Overview on Flight Controllers for Autonomous Rotorcraft

Although much progress has been made in autonomous flight [8,9], the reported controllers have achieved quite modest performance. The flight modes are generally limited to hover and low-speed straight flight. This may be attributed to many factors, such as parametric uncertainty, unmodeled dynamics, actuator magnitude saturation, model nonlinearities, external disturbances, sensors noise, etc. The design of a controller that deals with all these issues is very difficult and is still a challenge for researchers. Therefore, designers often focus on a specific problem, thereby resulting in various techniques such as the differential-flatness approach [10–12], backstepping methodology [5,13], adaptive control [14], robust control [15], small-gain methods [1], etc. The work in [7] summarizes different control techniques, including both control architectures and control methods for UAVs.

The effects of parametric uncertainty and unmodeled dynamics have been handled using system identification [16] or robust control techniques [15,17]. A robust H_∞ loop-shaping controller [15] has been implemented and tested on a robotic helicopter, thereby providing some robustness with respect to unmodeled dynamics. The obtained results are very satisfactory. However, robust control using H_∞ is known to be conservative and presents tradeoffs between performance and robustness. Furthermore, the controller design employs a linearized model extracted at hover. Thus, degradation of the performance is expected when the helicopter executes aggressive maneuvers.

Robust control design tools become inapplicable when modeling uncertainties are large. Adaptive control is then required to handle such large and time-varying uncertainties. Many adaptive controllers have been proposed for helicopter control [18–20]. Recently, adaptive controllers have been proposed [14] for trajectory tracking of a helicopter. Dynamic inversion and neural networks were used to compensate the modeling errors. Very promising results were obtained when implementing this controller on the R-Max helicopter. However, it requires overcoming important difficulties such as the presence of unstable zero dynamics that may lead to unstable control. Furthermore, global asymptotic stability of the system is lost due to the use of a linearized model and neural networks.

Actuator saturations limit the operational envelope of the vehicle to the region in which control designs are valid. They can also severely limit the achieved bandwidth of the system. Indeed, poor tracking performance and altitude oscillations due to actuator saturations have been reported [14]. Adaptive control has some inherent limitations that have been well recognized in the literature. Most notably, significant issues arise due to limitations on the plant inputs [21]. Input saturation is a problem for both adaptive and robust control [22]. Adaptive and robust control theories usually avoid issues related to input saturation and other system input characteristics by assumption. This conflicts with the fact that real systems, especially small UAVs, have these characteristics.

Moreover, the previously presented controllers [14,15] separate the flight control problem into an inner loop that controls attitude and an outer loop that controls the translational movement. Most of these control designs use an approximate linear model of the helicopter and assume the outer-loop bandwidth to be lower than that of the inner loop. This may result in degradation of the performance when the helicopter leaves the hovering position.

Most of the controllers proposed in the literature have been designed to cope with parametric uncertainties and unmodeled dynamics. The actuator saturation problem has not received as much attention. Most controllers that do not consider the input saturation tend to fail [23], especially in aggressive maneuvers in which the vehicle operates near its limits.

B. Description of the Proposed Control Law

Small rotary-wing UAVs are very sensitive to actuator saturation. In view of payload constraints, the vehicle's motors are chosen such that the rotorcraft operates near its physical limits. Furthermore, small UAVs are designed to fly close to the ground in complex and cluttered environments. Therefore, the UAV may execute aggressive maneuvers to avoid obstacles. So actuator saturation occurs frequently due to aggressive maneuvers or external disturbances. Thus, actuator saturation is particularly prevalent and has a significant effect on the overall stability of small aircraft.

Several new nonlinear tools have been introduced for analyzing and controlling linear and nonlinear systems with saturation [24–29]. One of the fundamental methods is the *nested-saturation technique* [29,30], including its robust version [31]. This method was introduced for controlling a chain of integrators $x^{(n)} = u$ using a single bounded input $u \in [-u_{\max}, u_{\max}]$. Proposed was a nested-saturation-based control law of the form

$$u = -\sigma_{u_{\max}}(y_n + \sigma_{\frac{u_{\max}}{2}}[y_{n-1} + \ldots + \sigma_{\frac{u_{\max}}{2^{n-1}}}(y_1)])$$

which ensures global asymptotic stability of the closed-loop system while satisfying the constraints on control input magnitude, where $\sigma_{u_{\max}}(.)$ denotes a saturation function with a saturation limit $u_{\max}$, and the variables y_i are a linear combination of the state variables x_i. Exploiting this technique, a control strategy [1,4] has been proposed to stabilize a quadrotor aircraft with bounded inputs. The quadrotor rotorcraft has been considered as two independent planar vertical taking-off and landing (PVTOL) systems. The control strategy aimed at first stabilizing the altitude z, then the first PVTOL's angular displacement ϕ and y position, and finally, the second PVTOL's angular displacement θ and x position, without taking into account the coupling between these three subsystems [4,32].

The present paper extends these previous works [4,32]. The main contribution is the proof of global asymptotic stability for the complete model of the quadrotor helicopter, considering the coupling between the two PVTOLs and the influence of the altitude movement control on the horizontal (longitudinal and lateral) displacement. We also provide a convergence analysis for a large range of saturation levels. This allows us to have more flexibility in the adjustment of the controller and to reduce the time response of the closed-loop system. Moreover, gains have been added in the control law to improve the convergence speed of the closed-loop system and to guarantee the robustness against the nonlinear coupling terms. In addition, a real-time application with onboard controller and embedded sensors for position and attitude measurement is also presented.

Compared with previous controllers, our control strategy has particular advantages, such as global asymptotic stability of the rotorcraft nonlinear model with considering couplings between attitude and position. Furthermore, the actuator saturation is considered in the control design with ensuring fast convergence of the closed-loop system. In addition, we found that the nested-saturation control technique offers several advantages when applied to small rotorcraft. This type of control law is such that the input amplitude is smaller than the prespecified upper bound. Moreover, the nested structure of the control strategy simplifies the tuning of the flight controller parameters because there is a clear relationship between the parameters and the observed behavior in practice. Indeed, we first adjust the gains corresponding to the angular speed feedback, then we tune the parameters corresponding to the angular position feedback, and so forth. Another advantage of this type of control law is that it establishes a priority order between the different state variables. This means that the control law first stabilizes the angular speed and then, when the angular speed is low enough, it takes care of the angular position. Once the angular position is close to the horizontal, the controller attempts to reduce the linear horizontal displacement of the aircraft. Finally, once the helicopter has slowed down, it then starts to reach the desired horizontal position. Notice that it does not matter if the aircraft is too far from the desired position. It will not generate large control inputs when the

position error is large because such error is passed through a saturation function.

This paper is organized as follows. In Sec. II, we present the nonlinear model of a class of aerial vehicles. Section III considers the stabilization problem, and the convergence analysis of the closed-loop system is presented in Sec. IV. The dynamical performance of the proposed control law is compared in simulations to previous results [4] in Sec. V. Section VI is devoted to the testbed description and experiment setup. The paper ends with some conclusions in Sec. VII.

II. Rotorcraft's Nonlinear Model

The full model of a helicopter involving the flexibility of rotors, fuselage aerodynamics, and actuators dynamics is very complex [33,34]. In most cases, the aerial robot is considered as a rigid body evolving in a three-dimensional space. The equations of motion for a rigid body subject to external force $F^{\text{ext}} \in \mathbb{R}^3$ and torque $\tau \in \mathbb{R}^3$ applied to the center of mass and specified with respect to the body coordinate frame $\mathcal{B} = (X_\mathcal{B}, Y_\mathcal{B}, Z_\mathcal{B})$ are given by the following Newton–Euler equations in $\mathcal{B}$ [2,35,36]:

$$\begin{cases} m\dot{v}^{\mathcal{B}} + \Omega \times mv^{\mathcal{B}} = F^{\text{ext}} \\ J\dot{\Omega} + \Omega \times J\Omega = \tau \end{cases} \tag{1}$$

where F^{ext} consists of the gravity force and the lift vector F.

Let R be the rotation matrix from $\mathcal{B}$ to $\mathcal{I}$, which can be obtained using the convention XYZ and Euler angles $\eta = (\phi, \theta, \psi)$:

$$R = R_\phi \cdot R_\theta \cdot R_\psi = \begin{bmatrix} c_\theta c_\psi & c_\theta s_\psi & -s_\theta \\ s_\phi s_\theta c_\psi - c_\phi s_\psi & s_\phi s_\theta s_\psi + c_\phi c_\psi & s_\phi c_\theta \\ c_\phi s_\theta c_\psi + s_\phi s_\psi & c_\phi s_\theta s_\psi - s_\phi c_\psi & c_\phi c_\theta \end{bmatrix} \tag{2}$$

Note that R belongs to the *special orthogonal group* $SO(3)$ of all 3×3 orthogonal matrices that satisfy 1) $R^{-1} = R^T$ and 2) $\det(R) = 1$. By using this transformation, the first equation in Eq. (1), describing the translational dynamics, can be written in $\mathcal{I}$ [37]:

$$m\ddot{\xi} = RF - mgZ_\mathcal{I} \tag{3}$$

Let us recall the kinematic relationship [35] between the generalized velocities $\dot{\eta} = (\dot{\phi}, \dot{\theta}, \dot{\psi})$ and the angular velocity Ω:

$$\Omega = W\dot{\eta}, \qquad W \in \mathbb{R}^{3\times 3} \tag{4}$$

To exploit the nested-saturation technique that is generally applied to systems in feedforward structure, we will transform system (1) into a suitable structure. First, substituting Eqs. (3) and (4) into Eq. (1), and defining a pseudoinertia matrix $\mathbb{I}(\eta) = JW$ and a Coriolis vector $C(\dot{\eta}, \eta) = \dot{\mathbb{I}}\,\dot{\eta} + W\dot{\eta} \times \mathbb{I}\dot{\eta}$, we obtain

$$\begin{cases} m\ddot{\xi} = RF - mgZ_\mathcal{I} \\ \mathbb{I}(\eta)\ddot{\eta} + C(\dot{\eta}, \eta) = \tau \end{cases} \tag{5}$$

This model has the same structure as the system presented in [1,4] which is obtained using the Euler–Lagrange approach. The main difference is the expressions of $\mathbb{I}$ and C, which are more complex and more difficult to implement and to compute in the case of the Euler–Lagrange method. It is important to note that the model (5) is common for all aerial robots with six degrees of freedom.

Many rotary-wing UAVs can be characterized by three control torques $\tau = (\tau_\phi, \tau_\theta, \tau_\psi)^T$ and one control force $F = (0, 0, u)^T$. Then, by recalling Eq. (5), the dynamics of this class of rotorcraft are governed by

$$m\ddot{\xi} = u \begin{pmatrix} -s_\theta \\ s_\phi c_\theta \\ c_\phi c_\theta \end{pmatrix} + \begin{pmatrix} 0 \\ 0 \\ -mg \end{pmatrix} \tag{6}$$

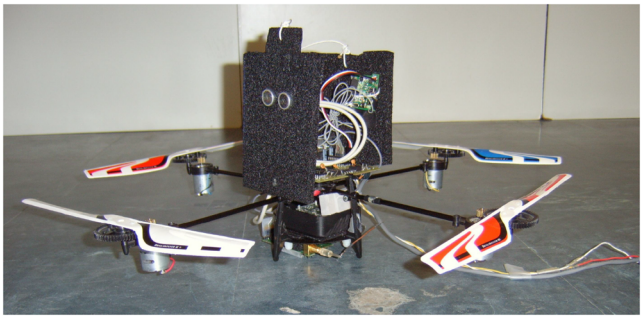

Fig. 1 Instrumented Draganflyer rotorcraft.

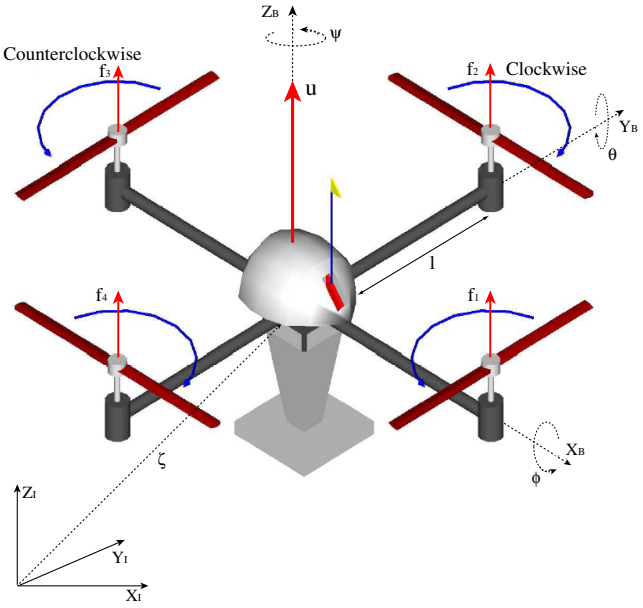

Fig. 2 Quadrotor aircraft configuration.

$$\mathbb{I}(\eta)\ddot{\eta} = \tau - C(\dot{\eta}, \eta) \tag{7}$$

The analytical expressions of the four control inputs $(u, \tau_\phi, \tau_\theta, \tau_\psi)$ depend on the rotorcraft configuration and the mechanism for generating these moments and forces.

The quadrotor-based mechanism is generally used for small UAVs such as the Draganfly rotorcraft (see Fig. 1). The front and the rear motors rotate counterclockwise while the other two motors rotate clockwise. As a result, gyroscopic effects and aerodynamic torques tend to cancel in trimmed flight. The gyroscopic moments that occur when rotors are not spinning at exactly the same speed can be neglected. In the following, we include the relations between the control inputs and the motor velocities in the case of the quadrotor aircraft (see Fig. 2). The collective lift u is the sum of the thrusts generated by the four propellers [33]:

$$u = \sum_{i=1}^{4} f_i = \sum_{i=1}^{4} \mu w_i^2$$

In fact, propeller thrust and torque are generally assumed to be proportional to the square of the angular velocity.

The airframe torques generated by the rotors are given by [1]

$$\tau_\phi = l\mu\left(w_2^2 - w_4^2\right) \tag{8}$$

$$\tau_\theta = l\mu\left(w_3^2 - w_1^2\right) \tag{9}$$

$$\tau_\psi = \kappa\left(w_1^2 + w_3^2 - w_2^2 - w_4^2\right) \tag{10}$$

where μ and κ are positive constants characterizing the propellers aerodynamics. In fact, the relation between the rotor angular velocity w and the generated lift is very complex [33,37]. The expressions in Eqs. (8–10) are valid approximations that we find in the literature of helicopters and that are used in cases of hovering and low-speed displacements.

Furthermore, the airframe is subject to additional torques due to the motor's acceleration. Thus, the equation giving the yawing moment is slightly modified as follows:

$$\tau_\psi = \kappa\left(w_1^2 + w_3^2 - w_2^2 - w_4^2\right) + I_p(\dot{w}_1 + \dot{w}_3 - \dot{w}_2 - \dot{w}_4) \tag{11}$$

Now we can represent the relations between the control inputs and motor velocities as

$$\begin{pmatrix} u \\ \tau_\phi \\ \tau_\theta \\ \tau_\psi \end{pmatrix} = \begin{pmatrix} \mu & \mu & \mu & \mu \\ 0 & l\mu & 0 & -l\mu \\ -l\mu & 0 & l\mu & 0 \\ \kappa & -\kappa & \kappa & -\kappa \end{pmatrix} \begin{pmatrix} w_1^2 \\ w_2^2 \\ w_3^2 \\ w_4^2 \end{pmatrix} + \begin{pmatrix} 0 & 0 & 0 & 0 \\ 0 & 0 & 0 & 0 \\ 0 & 0 & 0 & 0 \\ I_p & -I_p & I_p & -I_p \end{pmatrix} \begin{pmatrix} \dot{w}_1 \\ \dot{w}_2 \\ \dot{w}_3 \\ \dot{w}_4 \end{pmatrix} \tag{12}$$

Unlike standard helicopters, the main thrust and control torques are obtained by controlling the angular speed of the four rotors without using any servomechanism. So the construction and the maintenance of the quadrotor aircraft is relatively simple when compared with other rotorcraft configurations. However, the motors operate near their maximum speed. Therefore, the control law should consider actuator saturation to prevent the control system from instabilities.

The control law presented in Sec. IV computes the control inputs $(u, \tau_\phi, \tau_\theta, \tau_\psi)$, and the corresponding motor velocities (w_1, w_2, w_3, w_4) are then deduced from Eq. (12). By neglecting the small motor accelerations and solving system (12), the bounds on thrust and torques are mapped into the bounds on rotors speeds as follows:

$$\begin{cases} w_{1_{\max}} & = w_{3_{\max}} = \frac{1}{2}\sqrt{u_{\max} + \tau_{\psi_{\max}} + 2\tau_{\theta_{\max}}} \\ w_{2_{\max}} & = w_{4_{\max}} = \frac{1}{2}\sqrt{u_{\max} + \tau_{\psi_{\max}} + 2\tau_{\phi_{\max}}} \end{cases} \tag{13}$$

The bounds on thrust and torques can be chosen such that they satisfy the constraints in Eq. (13). Therefore, one avoids a situation in which the four rotors are spinning at maximum speed to keep the vehicle in hover, leaving no authority available for pitch and roll control while maintaining altitude. Indeed, the nested-saturation-based control law can handle this problem by choosing the bound on u to be smaller than the real available thrust, thereby leaving authority for pitch and roll control. From Eq. (13), we can see that when the thrust reaches its maximum value $u_{\max}$, the rotors are not spinning at their maximum speed $w_{\max}$. Thus, pitch and roll torques can be obtained even if the thrust u is saturated. However, if the external disturbances such as wind are relatively large, then it would be difficult to control the attitude while keeping the same altitude, because of aircraft capabilities. Indeed, this problem is independent of the used controller; rather, it concerns the limitations of the physical system.

III. Stabilization with Bounded Inputs

The quadrotor aircraft has a nonlinear underactuated (i.e., has more state variables than control inputs) dynamic model [Eqs. (6) and (7)] in which the rotation and the translation are coupled through the matrix R. The proposed framework for stabilizing the underactuated system [Eqs. (6) and (7)] while considering the input boundedness and translation-rotation coupling is the design of a robust controller using a forwarding approach. In fact, our control strategy takes advantage of the structure of the quadrotor configuration model and it is based on the nested-saturation technique. Control inputs and state variables are then sequentially bounded in an appropriate priority order. This control law is motivated by its ability to handle coupling terms between rotation and translation as well as input boundedness.

Let us first consider the following change of variables:

$$\tau = C(\eta, \dot{\eta}) + \mathbb{I}\tilde{\tau} \tag{14}$$

where

$$\tilde{\tau} = \begin{pmatrix} \tilde{\tau}_\phi \\ \tilde{\tau}_\theta \\ \tilde{\tau}_\psi \end{pmatrix}$$

are the new control torques. Replacing τ in Eq. (7) by its expression given in Eq. (14), Eq. (7) becomes linear because we compensated the Coriolis vector. Indeed, we obtain

$$\ddot{\eta} = \tilde{\tau} \tag{15}$$

Using Eqs. (6) and (15), the rotary-wing aircraft model can be represented by the following system:

$$\begin{cases} m\ddot{x} & = -u\sin\theta \\ m\ddot{y} & = u\cos\theta.\sin\phi \\ m\ddot{z} & = u\cos\theta.\cos\phi - mg \\ \ddot{\phi} & = \tilde{\tau}_\phi \\ \ddot{\theta} & = \tilde{\tau}_\theta \\ \ddot{\psi} & = \tilde{\tau}_\psi \end{cases} \tag{16}$$

We notice that this system can be divided into four coupled subsystems that are controlled by a single input to each one. We then propose the following control strategy:

1) Control the altitude z by the total thrust u.

2) Use the torque $\tilde{\tau}_\psi$ to control the yaw angle ψ.

3) Stabilize the horizontal movement ($\theta - x$ and $\phi - y$) by the remaining control inputs $(\tilde{\tau}_\theta, \tilde{\tau}_\phi)$.

In the following, we propose a nonlinear controller for each subsystem, and we prove that the proposed control law takes into account the coupling terms connecting these subsystems. Indeed, we consider the effects of coupling terms as disturbances. Thus, we propose a decoupled control design and provide a complete stability analysis of the closed-loop system. In the proposed controller, integral action to handle steady-state disturbances cannot be added. However, we observed in simulations and experiments some kind of robustness against external disturbances with such methodology.

A. Yaw and Altitude Control

The yaw dynamic is governed by the following double integrator:

$$\ddot{\psi} = \tilde{\tau}_\psi$$

The nested-saturation-based control scheme [29] ensures global asymptotic stability of a general system composed of n integrators in cascade. Therefore, the control law

$$\tilde{\tau}_\psi = -\sigma_{\psi_1}(k_{\psi_1}\dot{\psi} + \sigma_{\psi_2}[k_{\psi_2}\dot{\psi} + k_{\psi_1}k_{\psi_2}(\psi - \psi_d)]) \tag{17}$$

will stabilize the yaw angle at its desired value ψ_d if the positive gains (k_{ψ_1}, k_{ψ_2}) are well-chosen [38], where $\sigma(.)$ is a linear saturation function that is Lipchitz, nondecreasing, and defined as $\sigma_{\psi_i}(x) = \text{sign}(x)\min(|x|, \psi_i)$, $(i = 1, 2)$, and ψ_i is a real positive constant.

Now we consider the equation describing the altitude dynamic:

$$m\ddot{z} = u\cos\theta\cos\phi - mg$$

First, we apply a feedback linearization [32] by assigning

$$u = \frac{mr + mg}{\cos\sigma_p(\theta)\cos\sigma_p(\phi)} \tag{18}$$

where $0 < p < \pi/2$. We assume that after a finite time, both $\theta(t)$ and $\phi(t)$ belong to the interval

$$I_{\pi/2} = \left(-\frac{\pi}{2} + \epsilon, \frac{\pi}{2} - \epsilon\right)$$

for some $\epsilon > 0$, so that $\cos\theta\cos\phi \neq 0$.

Then, we obtain a double integrator system:

$$\ddot{z} = r$$

where r is a new input.

As for the yaw control, we choose

$$r = -\sigma_{r_1}(k_{r_1}\dot{z} + \sigma_{r_2}[k_{r_2}\dot{z} + k_{r_1}k_{r_2}(z - z_d)]) \tag{19}$$

B. Horizontal Movement Control ($\theta - x$ and $\phi - y$)

After replacing u by its expression in Eq. (18), the remaining dynamics are given by

$$\begin{cases} \ddot{x} &= -\frac{r+g}{\cos\phi}\tan\theta \\ \ddot{y} &= (r+g)\tan\phi \\ \ddot{\phi} &= \tilde{\tau}_\phi \\ \ddot{\theta} &= \tilde{\tau}_\theta \end{cases} \tag{20}$$

System (20) can be seen as two feedforward subsystems ($x - \theta$ and $y - \phi$) coupled by the term $\cos\phi$ and controlled by $\tilde{\tau}_\theta$ and $\tilde{\tau}_\phi$, respectively. The variable r can be considered as a bounded ($|r| \leqslant r_1$) perturbation for system (20).

We denote $|X| \in \mathbb{R}^n$ as a positive vector that is composed of the absolute value of each component of X, that is, $|X| = (|x_1|, |x_2|, \ldots, |x_n|)^T$. In the following sections, for $|X| \in \mathbb{R}^n$ and $|Y| \in \mathbb{R}^n$, the notation $|X| > (<)|Y|$ means that $|x_i| > (<)|y_i|$, $\forall\ i \in \{1, 2, \ldots, n\}$.

We denote $\tilde{\xi} = (x, y)^T$ as the position vector and $\tilde{\eta} = (\theta, \phi)^T$ denotes the orientation vector.

We define a vector saturation function σ_a:$\mathbb{R}^2 \to \mathbb{R}^2$ as

$$\sigma_a(X) = [\sigma_{a_1}(x_1), \sigma_{a_2}(x_2)]^T$$

where a_1 and a_2 are real positive constants that define the saturation levels of $\sigma(.)$.

Using these notations, system (20) can be written in the form

$$\begin{cases} \dot{\tilde{\xi}} &= A\tilde{\eta} + D(\tilde{\eta}, r) \\ \ddot{\tilde{\eta}} &= \nu \end{cases} \tag{21}$$

where

$$A = \begin{pmatrix} -g & 0 \\ 0 & g \end{pmatrix}, \qquad \nu = (\tilde{\tau}_\theta, \tilde{\tau}_\phi)^T$$

and

$$D(\tilde{\eta}, r) = \begin{pmatrix} -(r+g)\frac{\tan\theta}{\cos\phi} + g\theta \\ (r+g)\tan\phi - g\phi \end{pmatrix} \tag{22}$$

System (21) can be seen as a chain of four integrators according to the variables $\tilde{\xi}$ and $\tilde{\eta}$, which is perturbed by the nonlinear function $D(\tilde{\eta}, r)$.

Thus, the control law ν will be constructed recursively in four steps. The key idea is to bound each variable successively, starting with $\dot{\tilde{\eta}}$. The boundedness is obtained by choosing suitable control inputs containing saturating functions and using the Lyapunov analysis. Then, when the nonlinear coupling term $D(\tilde{\eta}, r)$ is small, the convergence property of the system is guaranteed by appropriately selecting the saturation levels.

1. *Boundedness of* $\dot{\tilde{\eta}}$

We first examine the trajectory of $\dot{\tilde{\eta}}$. We recall

$$\dddot{\tilde{\eta}} = \nu \tag{23}$$

Let us define V_1, a positive definite function

$$V_1 = \tfrac{1}{2}\dot{\tilde{\eta}}^T\dot{\tilde{\eta}}$$

for which the time derivative may be written as

$$\dot{V}_1 = \dot{\tilde{\eta}}^T\ddot{\tilde{\eta}} = \dot{\tilde{\eta}}^T\nu \tag{24}$$

The input ν is chosen as follows:

$$\nu = -\sigma_a[K_1\dot{\tilde{\eta}} + \sigma_b(\nu_1)] \tag{25}$$

where $\nu_1 \in \mathbb{R}^2$ is the new input that will be assigned in the next step, and $K_1 \in \mathbb{R}^{2\times 2}$ is a diagonal gain matrix composed of positive constants, that is,

$$K_1 = \begin{pmatrix} k_{1_\theta} & 0 \\ 0 & k_{1_\phi} \end{pmatrix}$$

Now we have

$$\dot{V}_1 = -\dot{\tilde{\eta}}^T\sigma_a[K_1\dot{\tilde{\eta}} + \sigma_b(\nu_1)]$$

It is clear that if $|K_1\dot{\tilde{\eta}}| > b$, then $\dot{V}_1 < 0$ and $\dot{\tilde{\eta}}$ will decrease until it reaches the domain of attraction $Q_1 = [-|K_1^{-1}b|, |K_1^{-1}b|]$. If the system starts outside Q_1, the trajectory of the derivative of $\tilde{\eta}$ eventually enters Q_1 in a finite time T_1 [1].

$$|K_1\dot{\tilde{\eta}}| \leqslant b, \quad \forall\ t \geqslant T_1 \tag{26}$$

If we choose $b \leqslant \frac{1}{2}a$, then σ_a will operate in its linear region for all $t \geqslant T_1$. Thus, Eq. (23) becomes

$$\dddot{\tilde{\eta}} + K_1\ddot{\tilde{\eta}} = -\sigma_b(\nu_1) \tag{27}$$

In the sequel, the matrices $K_i (i = 1, \ldots, 4) \in \mathbb{R}^{2\times 2}$ are diagonal and composed of positive constants k_{i_θ} and k_{i_ϕ}.

2. *Boundedness of* $\tilde{\eta}$

Now we consider the new system in Eq. (27) with the new input ν_1. By defining a new variable z_2 such as

$$z_2 = \ddot{\tilde{\eta}} + K_1\dot{\tilde{\eta}} \tag{28}$$

then we have $\dot{z}_2 = -\sigma_b(\nu_1)$.

We continue the process by choosing

$$\nu_1 = K_2 z_2 + \sigma_c(\nu_2) \tag{29}$$

The time derivative of z_2 is then given by

$$\dot{z}_2 = -\sigma_b[K_2 z_2 + \sigma_c(\nu_2)] \tag{30}$$

which is similar to $\dddot{\tilde{\eta}}$ in Eqs. (23) and (25). As done previously, we define a positive definite function V_2 as

$$V_2 = \tfrac{1}{2}z_2^T z_2$$

Then

$$\dot{V}_2 = z_2^T\dot{z}_2 = -z_2^T\sigma_b[K_2 z_2 + \sigma_c(\nu_2)]$$

The control law (29) forces the variable z_2 to converge to its domain of attraction in a finite time $T_2 \geqslant T_1$, that is,

$$|K_2 z_2| \leqslant c, \quad \forall\ t \geqslant T_2 \tag{31}$$

By setting $c \leqslant \frac{1}{2}b$, system (30) becomes

$$\dot{z_2} + K_2 z_2 = -\sigma_c(\nu_2) \tag{32}$$

The boundedness of $\tilde{\eta}$ ($\tilde{\eta} \in Q_{\tilde{\eta}}$) can be deduced by solving the differential Eq. (28) for $t \geqslant T_2$.

$$\tilde{\eta}(t) = \tilde{\eta}(T_2)e^{-K_1(t-T_2)} + \int_{T_2}^{t} e^{-K_1(t-\delta)} z_2(\delta)\, \mathrm{d}\delta \tag{33}$$

Therefore, it follows that there exists a finite time $T_3 \geqslant T_2$ such that for $t \geqslant T_3$, we have [32]

$$|K_2\tilde{\eta}| \leqslant c, \quad \forall\ t \geqslant T_3 \tag{34}$$

Notice that $Q_{\tilde{\eta}}$ depends on c and K_2. Therefore, the parameters c and K_2 can be chosen to guarantee that $\tilde{\eta} \in I_{\pi/2} \times I_{\pi/2}$ for all $t \geqslant T_3$.

3. Boundedness of $\dot{\tilde{\xi}}$

Let us recall that

$$\begin{cases} \ddot{\tilde{\xi}} = A\tilde{\eta} + D(\tilde{\eta}, r) \\ \dot{z}_2 + K_2 z_2 = -\sigma_c(\nu_2) \\ z_2 = \dot{\tilde{\eta}} + K_1\tilde{\eta} \end{cases} \tag{35}$$

We define a new variable z_3 as follows:

$$z_3 = z_2 + K_2\tilde{\eta} + K_2K_1A^{-1}\dot{\tilde{\xi}} \tag{36}$$

Differentiating the preceding equation, we obtain

$$\begin{aligned} \dot{z}_3 &= \dot{z_2} + K_2\dot{\tilde{\eta}} + K_2K_1A^{-1}A\tilde{\eta} + K_2K_1A^{-1}D(\tilde{\eta}, r) \\ &= -\sigma_c(\nu_2) + K_2K_1A^{-1}D(\tilde{\eta}, r) \end{aligned} \tag{37}$$

The input ν_2 of this system is selected as $\nu_2 = K_3 z_3 + \sigma_d(\nu_3)$. Define a new positive definite function:

$$V_3 = \tfrac{1}{2}z_3^T z_3$$

The time derivative of V_3 can be written in the form

$$\dot{V}_3 = z_3^T\dot{z}_3 = -z_3^T\{\sigma_c[K_3 z_3 + \sigma_d(\nu_3)] - K_2K_1A^{-1}D(\tilde{\eta}, r)\}$$

Using a similar analysis, it can be shown that after a finite time $T_4 \geqslant T_3$, the variable z_3 satisfies

$$|K_3 z_3| \leqslant d + K_2K_1M, \quad \forall\ t \geqslant T_4 \tag{38}$$

where $M \in \mathbb{R}^2$ is a positive vector that is defined as follows [see Eqs. (61) and (62) for its explicit expression]:

$$M = \max_{(\tilde{\eta} \in Q_{\tilde{\eta}})} |A^{-1}D(\tilde{\eta}, r)| \tag{39}$$

From Eqs. (31), (34), (36), and (38), we can show that $\dot{\tilde{\xi}}$ is bounded.

If the saturation level c is chosen such that it satisfies

$$c \geqslant 2d + K_2K_1M$$

then $\dot{z}_3$ in Eq. (37) is given by

$$\dot{z}_3 + K_3 z_3 = -\sigma_d(\nu_3) + K_2K_1A^{-1}D(\tilde{\eta}, r) \tag{40}$$

4. Boundedness of $\tilde{\xi}$

Finally, the input ν_3 is chosen as follows:

$$\nu_3 = K_4(z_3 + K_3\tilde{\eta} + K_3(K_1 + K_2)A^{-1}\dot{\tilde{\xi}} + K_3K_2K_1A^{-1}\tilde{\xi}) \tag{41}$$

This choice is motivated by the fact that using Eqs. (35), (36), and (40), $\dot{\nu_3}$ can now be expressed as

$$\dot{\nu}_3 = -K_4[\sigma_d(\nu_3) - (K_3K_1 + K_3K_2 + K_2K_1)A^{-1}D(\tilde{\eta}, r)] \tag{42}$$

Let us define V_4 a positive definite function given by

$$V_4 = \tfrac{1}{2}\nu_3^T\nu_3$$

$\dot{V}_4$ is therefore

$$\begin{aligned} \dot{V}_4 = \nu_3^T\dot{\nu}_3 = -\nu_3^T K_4[&\sigma_d(\nu_3) \\ &- (K_3K_1 + K_3K_2 + K_2K_1)A^{-1}D(\tilde{\eta}, r)] \end{aligned}$$

If $d \geqslant (K_3K_1 + K_3K_2 + K_2K_1)M$, then after a finite time T_5, we obtain

$$|\nu_3| \leqslant (K_3K_1 + K_3K_2 + K_2K_1)M \leqslant d, \quad \forall\ t \geqslant T_5 \tag{43}$$

Therefore, Eq. (42) leads to

$$\dot{\nu}_3 + K_4\nu_3 = K_4(K_3K_1 + K_3K_2 + K_2K_1)A^{-1}D(\tilde{\eta}, r) \tag{44}$$

Because $\dot{\tilde{\xi}}$, $\tilde{\eta}$, z_3, and ν_3 are bounded $\forall\ t \geqslant T_5$, we conclude from Eq. (41) that $\tilde{\xi}$ is bounded. Thus, at this stage, we have bounded all the state variables, and all the saturation functions will operate in their linear regions for all $t \geqslant T_5$.

IV. Convergence Analysis

In this section, we will prove that all the state variables converge to zero, even in the presence of the nonlinear coupling term $D(\tilde{\eta}, r)$. The global asymptotic stability is ensured by a convenient choice of the saturation level c and the gains K_i.

Equation (44) can be written as follows:

$$\dot{\nu}_3 + K_4\nu_3 = KA^{-1}D(\tilde{\eta}, r) \tag{45}$$

where $K = K_4(K_3K_1 + K_3K_2 + K_2K_1)$.

The vector $A^{-1}D(\tilde{\eta}, r)$ can be subdivided into two terms: $H(\tilde{\eta})$, which depends only on the state vector $\tilde{\eta}$, and $R(\tilde{\eta}, r)$, which is function of $\tilde{\eta}$ and r. These vectors can be computed from Eq. (22) and expressed as

$$H(\tilde{\eta}) = \begin{pmatrix} \frac{\tan\theta}{\cos\phi} - \theta \\ \tan\phi - \phi \end{pmatrix}, \qquad R(\tilde{\eta}, r) = \begin{pmatrix} \frac{r\tan\theta}{g\cos\phi} \\ \frac{r\tan\phi}{g} \end{pmatrix} \tag{46}$$

Now Eq. (45) can be written in the form

$$\dot{\nu}_3 + K_4\nu_3 = KH(\tilde{\eta}) + KR(\tilde{\eta}, r)$$

After analyzing the preceding differential equation, we found that its solution satisfies the following inequality for all $\tilde{\eta} \in Q_{\tilde{\eta}}$:

$$|\nu_3| \leqslant K|H(\tilde{\eta})| + K|R(\tilde{\eta}, r)| \tag{47}$$

From Eq. (40), we also have

$$\dot{z}_3 + K_3 z_3 = -\nu_3 + K_2K_1H(\tilde{\eta}) + K_2K_1R(\tilde{\eta}, r)$$

Similarly,

$$|z_3| \leqslant (K + K_2K_1)(|H(\tilde{\eta})| + |R(\tilde{\eta}, r)|) \tag{48}$$

Because $\nu_2 = K_3 z_3 + \nu_3$, this implies that

$$|\nu_2| \leqslant [K + K_3(K + K_2K_1)][|H(\tilde{\eta})| + |R(\tilde{\eta}, r)|] \tag{49}$$

For simplicity, let us note that $K_0 = [K + K_3(K + K_2K_1)]$, which is a diagonal matrix.

Let us recall from Eq. (32) that $\dot{z}_2 + K_2 z_2 = -\nu_2$. We then deduce that

$$|z_2| \leqslant K_0|H(\tilde{\eta})| + K_0|R(\tilde{\eta}, r)| \tag{50}$$

Finally, the solution of the differential equation in Eq. (28) also satisfies

$$|\tilde{\eta}| \leqslant K_0|H(\tilde{\eta})| + K_0|R(\tilde{\eta}, r)| \tag{51}$$

Now we will prove that $\tilde{\eta}$ will converge to zero if the saturation level c is selected to be sufficiently small. By recalling Eqs. (34) and (51), one may write

$$\begin{cases} |\tilde{\eta}| \leqslant K_0|H(\tilde{\eta})| + K_0|R(\tilde{\eta}, r)| \\ K_2|\tilde{\eta}| \leqslant c \end{cases} \tag{52}$$

From Eqs. (46) and (52), we obtain

$$\begin{cases} |\theta| - k_{0_\theta}\left|\frac{\tan\theta}{\cos\phi} - \theta\right| \leqslant k_{0_\theta}\left|\frac{r\tan\theta}{g\cos\phi}\right| \\ k_{2_\theta}|\theta| \leqslant c_\theta \\ |\phi| - k_{0_\phi}|\tan\phi - \phi| \leqslant k_{0_\phi}\left|\frac{r\tan\phi}{g}\right| \\ k_{2_\phi}|\phi| \leqslant c_\phi \end{cases} \tag{53}$$

Because $0 < \cos\phi \leqslant 1$, then

$$\frac{\tan\theta}{\cos\phi}$$

and θ have the same sign, and we can easily verify that $|\tan\theta| \geqslant |\theta|$, which implies that

$$\left|\frac{\tan\theta}{\cos\phi}\right| \geqslant |\theta|$$

These remarks remain valid for the third inequality in Eq. (53) with the variable ϕ.

We conclude from these remarks that

$$\left|\frac{\tan\theta}{\cos\phi} - \theta\right| = \frac{|\tan\theta|}{\cos\phi} - |\theta| \qquad |\tan\phi - \phi| = |\tan\phi| - |\phi| \tag{54}$$

Furthermore, we have $k_{2_\phi}|\phi| \leqslant c_\phi$, then

$$\cos(c_\phi/k_{2_\phi}) \leqslant \cos\phi \leqslant 1 \Rightarrow 1 \leqslant \frac{1}{\cos\phi} \leqslant \frac{1}{\cos(c_\phi/k_{2_\phi})}$$

Substituting Eq. (54) into Eq. (53) and using the preceding inequality, we obtain

$$\begin{cases} (1 + k_{0_\theta})|\theta| - k_{0_\theta}\frac{\tan|\theta|}{\cos(c_\phi/k_{2_\phi})} \leqslant k_{0_\theta}|r|\frac{\tan|\theta|}{g\cos\phi} \\ k_{2_\theta}|\theta| \leqslant c_\theta \\ (1 + k_{0_\phi})|\phi| - k_{0_\phi}\tan|\phi| \leqslant k_{0_\phi}|r|\frac{\tan|\phi|}{g} \\ k_{2_\phi}|\phi| \leqslant c_\phi \end{cases} \tag{55}$$

Let us note that L_θ is the limit of $|\theta|$ when the time goes to infinity, and L_ϕ is the limit of $|\phi|$. Because the functions

$$\frac{\tan|\theta|}{g\cos\phi}$$

and

$$\frac{\tan|\phi|}{g}$$

are bounded and $\lim_{t\to\infty} r = 0$ [see Eq. (19)], then we obtain from Eq. (55)

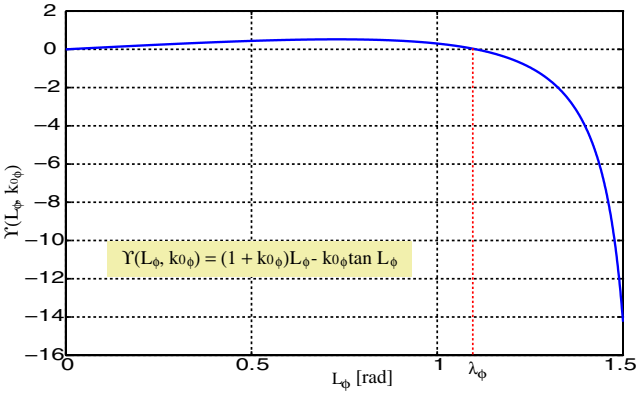

Fig. 3 Solution of inequality (56) for $k_{0_\phi} = 1.25$.

$$\begin{cases} (1 + k_{0_\theta})L_\theta - k_{0_\theta}\frac{\tan L_\theta}{\cos(c_\phi/k_{2_\phi})} \leqslant 0 \\ 0 \leqslant k_{2_\theta}L_\theta \leqslant c_\theta \\ (1 + k_{0_\phi})L_\phi - k_{0_\phi}\tan L_\phi \leqslant 0 \\ 0 \leqslant k_{2_\phi}L_\phi \leqslant c_\phi \end{cases} \tag{56}$$

Now, it remains to solve the algebraic system (56) for the variables L_θ and L_ϕ and to choose the saturation levels c_θ and c_ϕ sufficiently small to obtain $(L_\theta, L_\phi) = (0, 0)$.

By studying and plotting the inequality $(1 + k_{0_\phi})L_\phi - k_{0_\phi}\tan L_\phi \leqslant 0$, where $L_\phi \in \mathbb{R}^+$, we find that its solution is

$$0 \cup [\lambda_\phi, \frac{\pi}{2})$$

as shown in Fig. (3), in which λ_ϕ is a positive constant that depends on k_{0_ϕ}. Therefore, if we choose $c_\phi < k_{2_\phi}\lambda_\phi$ (i.e., $L_\phi < \lambda_\phi$), then the only possible solution is $L_\phi = 0$. We mention that λ_ϕ is inversely proportional to k_{0_ϕ}; this can be seen in the following example:

$$k_{0_\phi} \to 0 \Rightarrow \lambda_\phi \to \frac{\pi}{2} \qquad k_{0_\phi} = 1.25 \Rightarrow \lambda_\phi \simeq 1.105$$
$$k_{0_\phi} = 5 \Rightarrow \lambda_\phi \simeq 0.7 \qquad k_{0_\phi} = 7 \Rightarrow \lambda_\phi \simeq 0.6$$
$$k_{0_\phi} = 9 \Rightarrow \lambda_\phi \simeq 0.55 \qquad k_{0_\phi} \to \infty \Rightarrow \lambda_\phi \to 0$$

With the same analysis, we show that the solution of

$$(1 + k_{0_\theta})L_\theta - k_{0_\theta}\frac{\tan L_\theta}{\cos(c_\phi/k_{2_\phi})} \leqslant 0$$

is also

$$0 \cup [\lambda_\theta, \frac{\pi}{2})$$

where λ_θ is a positive constant that depends on the parameters c_ϕ, k_{2_ϕ}, and k_{0_θ}. As previously noted, there exists a value for $c_\theta (c_\theta < k_{2_\theta}\lambda_\theta)$ that restricts the solution to zero $(L_\theta = 0)$.

For example, if all of the gains are set to one (i.e., $K_i = I_{2\times 2}$ for $i = 1, \ldots, 4$), then, using Matlab, we obtain $k_{0_\phi} = k_{0_\theta} = 7$ and $L_\phi = 0$ if $c_\phi \leqslant 0.6$. Furthermore,

Table 1 Quadrotor model parameters

Model parameters	Values	Model parameters	Values
m, kg	1		
I_x, kg · m^2	5×10^{-3}	g, m/s^2	9.81
I_y, kg · m^2	5×10^{-3}	l, m	0.22
I_z, kg · m^2	9×10^{-3}	μ	3×10^{-6}
I_r, kg · m^2	4×10^{-5}	κ	1.5×10^{-7}

Table 2 Controller parameters

Controller parameters	Values	Controller parameters	Values
r_1	3	k_{r1}	1
r_2	1.4	k_{r2}	2
ψ_1	1.5	$k_{\psi 1}$	1
ψ_2	0.7	$k_{\psi 2}$	2
a_θ	1.7	k_{1_θ}	0.2
b_θ	0.82	k_{2_θ}	0.5
c_θ	0.36	k_{3_θ}	0.5
d_θ	0.16	k_{4_θ}	1.8
a_ϕ	1.7	k_{1_ϕ}	0.5
b_ϕ	0.82	k_{2_ϕ}	0.5
c_ϕ	0.4	k_{3_ϕ}	0.5
d_ϕ	0.18	k_{4_ϕ}	1

$$
\begin{aligned}
&\text{for } c_\phi = 0.6, \quad \text{if } c_\theta \leqslant 0, \quad \text{then } L_\theta = 0\\
&\text{for } c_\phi = 0.5, \quad \text{if } c_\theta \leqslant 0.09, \quad \text{then } L_\theta = 0\\
&\text{for } c_\phi = 0.45, \quad \text{if } c_\theta \leqslant 0.29, \quad \text{then } L_\theta = 0\\
&\text{for } c_\phi = 0.40, \quad \text{if } c_\theta \leqslant 0.38, \quad \text{then } L_\theta = 0\\
&\text{for } c_\phi = 0.35, \quad \text{if } c_\theta \leqslant 0.45, \quad \text{then } L_\theta = 0\\
&\text{for } c_\phi = 0.30, \quad \text{if } c_\theta \leqslant 0.49, \quad \text{then } L_\theta = 0\\
&\text{for } c_\phi = 0.2, \quad \text{if } c_\theta \leqslant 0.55, \quad \text{then } L_\theta = 0
\end{aligned}
$$

The objective is to choose c_ϕ and c_θ with high values to reduce the time convergence according to both axes x and y.

If we choose the gains k_i, as shown in Table 2, we find that for $c_\phi = 0.4 \Rightarrow L_\phi = 0$. Indeed, for these values, we have $k_{0_\phi} = 1.25$ and then $\lambda_\phi \simeq 1.105 \Rightarrow$, and we choose $c_\phi < k_{2_\phi}\lambda_\phi = 0.5 \times 1.105$.

Keeping these values and analyzing the inequality

$$(1 + k_{0_\theta})L_\theta - k_{0_\theta}\frac{\tan L_\theta}{\cos(c_\phi/k_{2_\phi})} \leqslant 0$$

we find that for $c_\theta \leqslant 0.36 \Rightarrow L_\theta = 0$.

Finally, we showed that the saturation level $c = (c_\theta, c_\phi)^T$ can be chosen in such a way that $\lim_{t\to\infty} \tilde{\eta} = 0$. We deduce from Eq. (46) that H and R converge to zero. From Eqs. (47–50), we have $(\nu_2, \nu_3, z_2, z_3) \to (0, 0, 0, 0)$. From the third equation of Eq. (35), we get $\dot{\tilde{\eta}} \to 0$. From Eqs. (36) and (41), it follows, respectively, that $\dot{\tilde{\xi}} \to 0$ and $\tilde{\xi} \to 0$.

A. Saturation Levels and Gain Matrices Selection

Let us recall all constraints on the saturation levels:

$$
\begin{cases}
a \geqslant 2b\\
b \geqslant 2c\\
c \geqslant 2d + K_2K_1M\\
d \geqslant (K_2K_1 + K_3K_1 + K_3K_2)M
\end{cases}
\tag{57}
$$

According to the previous section, c_θ and c_ϕ can be chosen as follows:

$$c_\phi = 0.4 \quad \text{and} \quad c_\theta = 0.36$$

Once the vector c is selected, the saturation levels a and b can be computed from Eq. (57). It remains to be shown how the saturation level d can be selected.

From Eq. (57), we get

$$(K_2K_1 + K_3K_1 + K_3K_2)M \leqslant d \leqslant \tfrac{1}{2}(c - K_2K_1M) \tag{58}$$

The vector d exists if the following condition holds:

$$(K_2K_1 + K_3K_1 + K_3K_2)M \leqslant \tfrac{1}{2}(c - K_2K_1M) \tag{59}$$

System (58) is equivalent to

$$
\begin{aligned}
&(k_{2_\theta}k_{1_\theta} + k_{3_\theta}k_{1_\theta} + k_{3_\theta}k_{2_\theta})M_\theta \leqslant d_\theta \leqslant \tfrac{1}{2}(c_\theta - k_{2_\theta}k_{1_\theta}M_\theta)\\
&(k_{2_\phi}k_{1_\phi} + k_{3_\phi}k_{1_\phi} + k_{3_\phi}k_{2_\phi})M_\phi \leqslant d_\phi \leqslant \tfrac{1}{2}(c_\phi - k_{2_\phi}k_{1_\phi}M_\phi)
\end{aligned}
\tag{60}
$$

From Eqs. (22) and (39), we have

$$M_\theta = \max_{\tilde{\eta}\in\Omega_{\tilde{\eta}}}\left|\frac{(r+g)}{g\cos(\phi)}\tan\theta - \theta\right| \qquad M_\phi = \max_{\phi\in\Omega_\phi}\left|\frac{(r+g)}{g}\tan\phi - \phi\right| \tag{61}$$

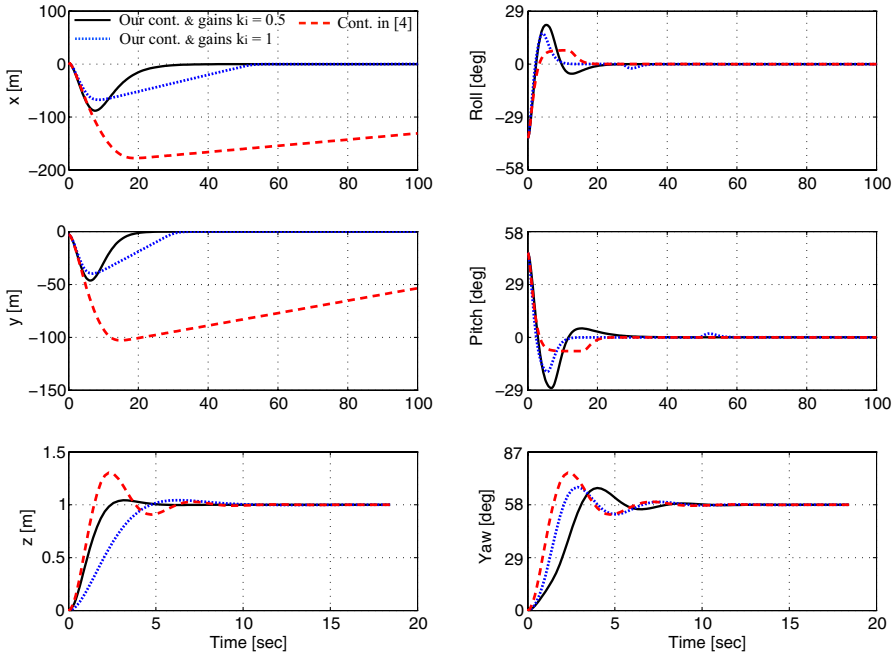

Fig. 4 Position and orientation stabilization.

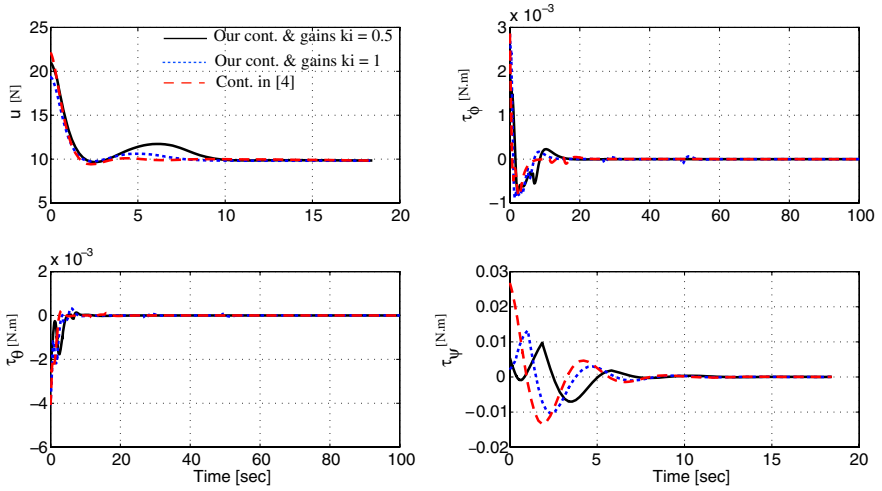

Fig. 5 Control inputs: total thrust and torques.

Because the perturbation $|r|$ is bounded by r_1 and for simplicity, we assume[¶] that $r_1 \geqslant 1$, then

$$M_\theta = \left| \frac{(r_1 + g)}{g \cos(c_\phi / k_{2_\phi})} \tan c_\theta - c_\theta \right| \qquad M_\phi = \left| \frac{(r_1 + g)}{g} \tan c_\phi - c_\phi \right| \tag{62}$$

First, the gain matrices K_i are selected by taking into account the following criteria. Obtain large values for c_θ and c_ϕ when solving the system (56). Satisfy the inequalities in Eq. (60) when selecting d_θ and d_ϕ. Finally, optimize the time response of the closed-loop system.

Considering the three preceding criteria, a primary analysis leads to the following selection of the matrices K_i. For $k_{i_\phi} = 0.5, i = 1,2,3$ and $k_{4_\phi} = 1$, and for $(k_{1_\theta}, k_{2_\theta}, k_{3_\theta}, k_{4_\theta}) = (0.2, 0.5, 0.5, 1.8)$, we obtain $c_\theta = 0.36$ and $c_\phi = 0.4$. Furthermore, if r_1 is set to three, then from Eq. (60), we obtain

$$0.1141 \leqslant d_\phi \leqslant 0.1810 \qquad 0.1555 \leqslant d_\theta \leqslant 0.1627$$

These gains and saturation levels values allowed the improvement of the dynamical performances of the closed-loop system (see Fig. 4). However, a detailed mathematical analysis is required to determine the best values for K_i that give a minimal time response of the system.

Finally, the complete expression of the control law is given by

$$\nu = -\sigma_a[K_1 \dot{\tilde{\eta}} + \sigma_b(K_2 z_2 + \sigma_c[K_3 z_3 + \sigma_d(\nu_3)])] \tag{63}$$

Replacing $(\tilde{\eta}, z_2, z_3, \nu_3)$ by their expressions [Eqs. (28), (36), and (41)], we obtain the complete formulas of the two control torques:

$$\begin{aligned} \tilde{\tau}_\theta = -\sigma_{a_\theta}\Bigg(& k_{1_\theta}\dot{\theta} + \sigma_{b_\theta}\Bigg\{ k_{2_\theta}(\dot{\theta} + k_{1_\theta}\theta) + \sigma_{c_\theta}\Bigg[k_{3_\theta}\Bigg(\dot{\theta} + (k_{1_\theta} \\ & + k_{2_\theta})\theta - k_{2_\theta}k_{1_\theta}\frac{\dot{x}}{g} \Bigg) + \sigma_{d_\theta}\Bigg(k_{4_\theta}\Bigg[\dot{\theta} + (k_{1_\theta} + k_{2_\theta} + k_{3_\theta})\theta \\ & - (k_{2_\theta}k_{1_\theta} + k_{3_\theta}k_{1_\theta} + k_{3_\theta}k_{2_\theta})\frac{\dot{x}}{g} - k_{3_\theta}k_{2_\theta}k_{1_\theta}\frac{x}{g} \Bigg] \Bigg) \Bigg] \Bigg\} \Bigg) \end{aligned} \tag{64}$$

and

$$\begin{aligned} \tilde{\tau}_\phi = -\sigma_{a_\phi}\Bigg(& k_{1_\phi}\dot{\phi} + \sigma_{b_\phi}\Bigg\{ k_{2_\phi}(\dot{\phi} + k_{1_\phi}\phi) + \sigma_{c_\phi}\Bigg[k_{3_\phi}\Bigg(\dot{\phi} + (k_{1_\phi} \\ & + k_{2_\phi})\phi + k_{2_\phi}k_{1_\phi}\frac{\dot{y}}{g} \Bigg) + \sigma_{d_\phi}\Bigg(k_{4_\phi}\Bigg[\dot{\phi} + (k_{1_\phi} + k_{2_\phi} + k_{3_\phi})\phi \\ & + (k_{2_\phi}k_{1_\phi} + k_{3_\phi}k_{1_\phi} + k_{3_\phi}k_{2_\phi})\frac{\dot{y}}{g} + k_{1_\phi}k_{2_\phi}k_{3_\phi}\frac{y}{g} \Bigg] \Bigg) \Bigg] \Bigg\} \Bigg) \end{aligned} \tag{65}$$

V. Simulations

Before testing the controller on the real system shown in Fig. 1, we performed different simulations in Matlab/Simulink using the dynamic model in Eq. (5) with the parameters listed in Table 1. The initial Euler angles and position are given by $\phi_0 = -40$ deg, $\theta_0 = 46$ deg, $\psi_0 = 0$ deg, $x_0 = 2$ m, $y_0 = -3$ m, and $z_0 = 0$ m. Linear and angular velocities are set to zero, that is, $\dot{\xi} = \dot{\eta} = (0,0,0)^T$. The task was to reach the position $z_d = 1$ m and $\psi_d = 58$ deg and to stabilize the other variables to zero. To explore the performance of the proposed controller, we run simulations for three controllers: the control law given by Eqs. (17), (19), (64), and (65) with gains $K_i = I_{2\times 2}$ (dashed/dotted-line curve), the same algorithm

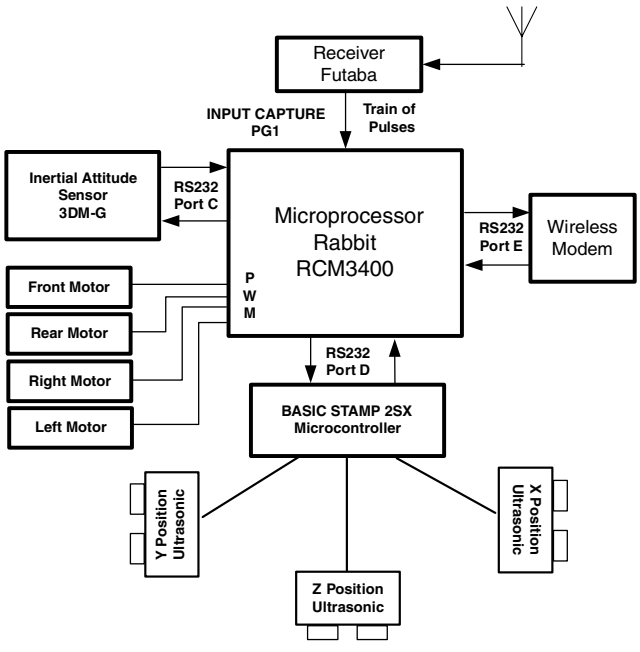

Fig. 6 Real-time architecture of the platform.

[¶]This assumption leads to simple expressions for M_θ and M_ϕ. However, one can compute M_θ and M_ϕ for any value of $r_1 > 0$. Notice also that in practice, r_1 may be $\geqslant 1$.

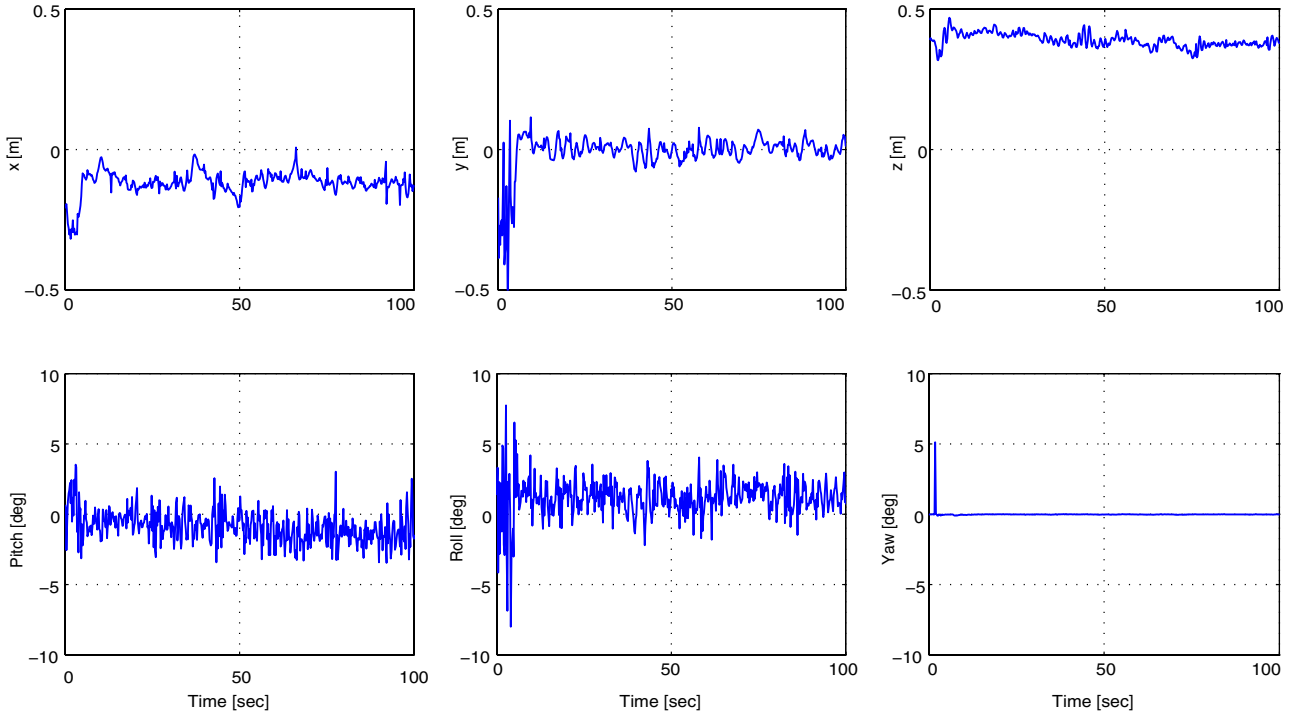

Fig. 7 Stabilization of the position and attitude of the helicopter.

with gains cut in half (solid-line curve, also see Table 2), and the third (dotted-line curve) represents previous controller results [4]. From Fig. 4, one can see that the x–y overshoots are reduced and the convergence speed of the state variables is improved with respect to the results obtained in [1,4]. Moreover, a convenient selection of saturation levels and gains K_i permits us to considerably reduce the time response of the system and to obtain satisfactory performance, as shown in Fig. 4. It is also important to note that the proposed control strategy increases the convergence speed without spending additional energy (also see [39] for comparison). Indeed, control input trajectories in Fig. 5 have almost the same behavior as previous results [1,4] and operate in the same amplitude range.

VI. Testbed and Experimental Results

The UAV platform used in the experiment is a modified Draganflyer III quadrotor helicopter (see Fig. 1) manufactured by Draganfly Innovations Inc. and is commercially available in Canada as a radio-controlled rotorcraft. It is approximately 0.75×0.75 m, fitted by four dc motors that are geared to the blades by a speed-reduction ratio of 5.6:1. In fact, we kept only the airframe, the motors, and the blades and added our own sensors and electronic circuitry.

The real-time architecture of the platform shown in Fig. 6 includes two microprocessors, a CI3DMGV MicroStrain inertial measurement unit (IMU), three ultrasonic sensors, a wireless modem, a Futaba 72-MHz radio, a receiver, a power MOSFET, and a ground station.

A microprocessor (Rabbit 3400, 28 MHz) is currently being used as the heart of the control system. The Rabbit 3400 is a fixed-point microcontroller, but the Dynamic C compiler emulates the floating-point operations. A second microcontroller (Pic) is added for the acquisition of the ultrasonic data and estimation of the robot position. These measurements are then sent to the Rabbit via RS-232. The IMU is mounted using a series of elastic bands such that low-amplitude, high-frequency vibrations of the helicopter cannot be transmitted to the sensor. The MicroStrain IMU uses a Kalman filter to fuse the rate gyro, accelerometer, and magnetometer data to generate pitch, roll, and heading (yaw) estimation at a frequency of 70 Hz. The angular velocities are also available. The Kalman filter is implemented internal to the IMU by the manufacturer. In our application, we directly use the IMU measurements without any filtering.

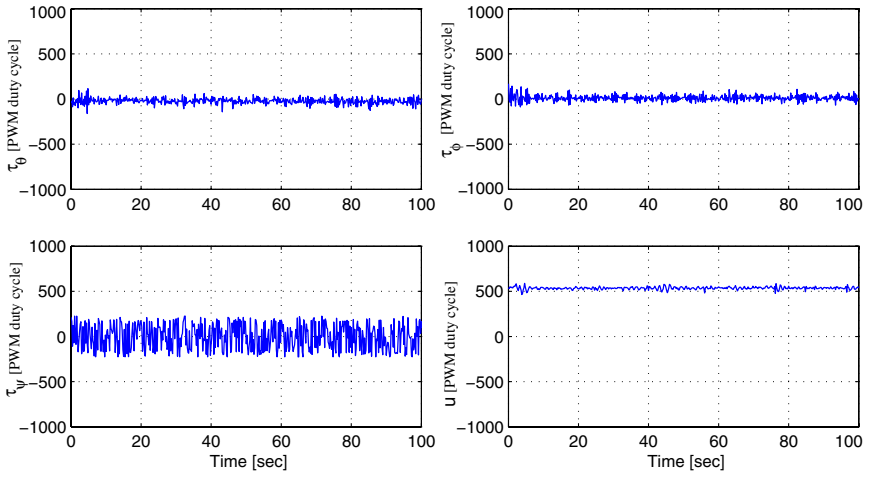

Fig. 8 Control inputs in the case of the stabilization problem.

Table 3 Statistical descriptors of state/input (PWM duty cycle) signals in the stabilization case

Variables	x, m	y, m	z, m	θ, deg	ϕ, deg	ψ, deg	τ_θ	τ_ϕ	τ_ψ	u
max	0.007	0.110	0.460	3.5	7.7	5.1	116	170	225	590
min	−0.310	−0.570	0.310	−3.4	−8.0	−0.1	−160	−88	−225	465
mean	−0.110	−0.007	0.380	−0.86	1.15	0.00	−22	11	−3	335
STD	0.043	0.067	0.024	1.13	1.35	0.22	34	35	142	14

The ultrasonic sensors operate at 20 Hz and are mounted according to the three axes to estimate the position $\xi = (x, y, z)^T$. We can then compute estimates of the linear velocities by using the approximation

$$\dot{\xi} = \frac{\xi(t) - \xi(t - T)}{T}$$

where T is the sampling period. In our experiment, $T = 0.05$ s, due to limitations imposed by the strategy used for estimating the position by the ultrasonic sensors. Both position and linear velocities are filtered using first-order low-pass filters.

Communication with the ground station is carried out via a 2.4-GHz wireless modem. The state variables and the control inputs are recovered, plotted, and analyzed in the ground station.

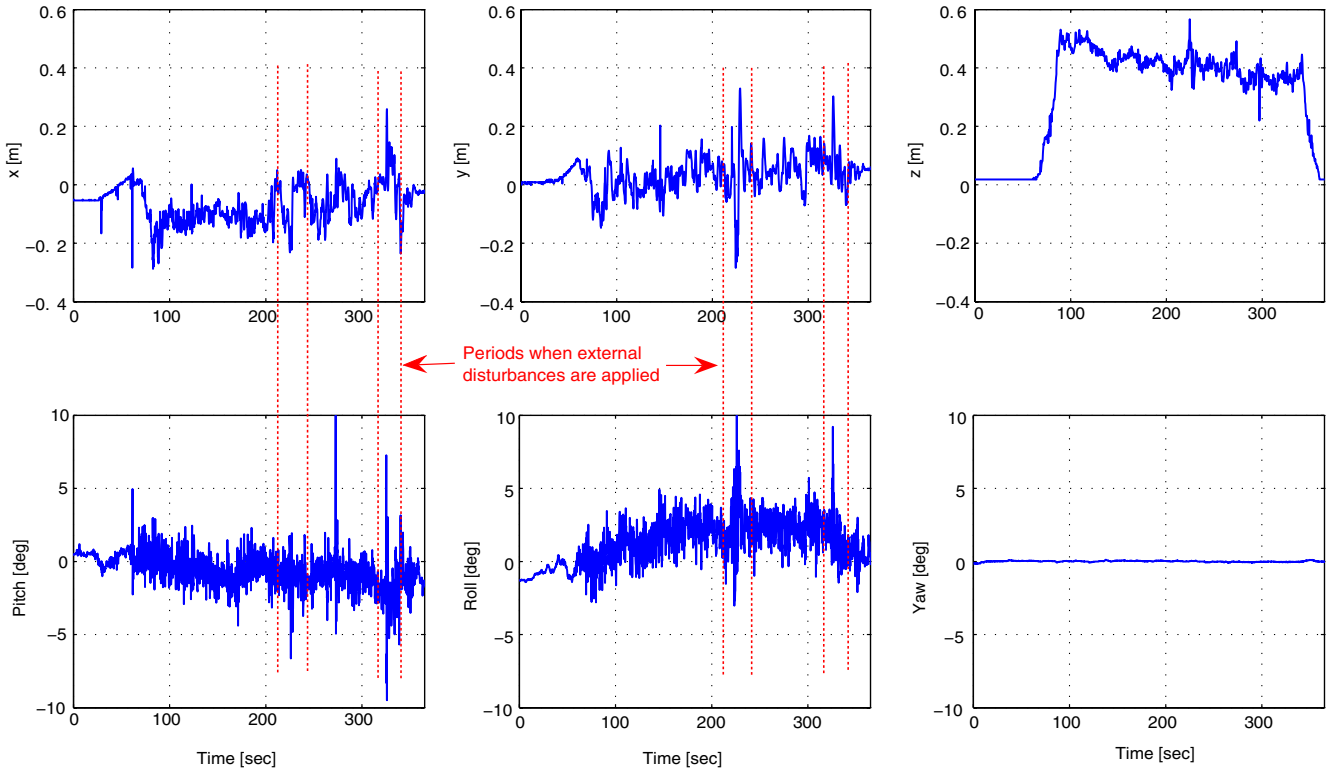

Fig. 9 Autonomous takeoff, hovering, and landing with external perturbations during the period 225 s–330 s.

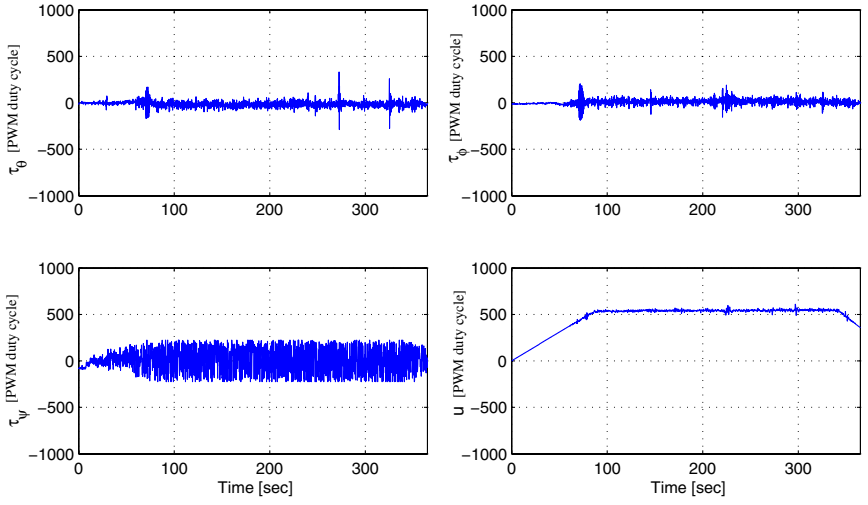

Fig. 10 Control inputs in terms of the pulse with modulation (PWM) duty cycle.

Table 4 Statistical descriptors of state/input (PWM duty cycle) signals in the case of autonomous flight

Variables	x, m	y, m	z, m	θ, deg	ϕ, deg	ψ, deg	τ_θ	τ_ϕ	τ_ψ	u
max	0.259	0.329	0.566	14.4	11.0	0.1	332	206	225	610
min	−0.288	−0.284	0.015	−9.4	−3.0	−0.1	−288	−187	−225	0
mean	−0.066	0.032	0.410	−0.5	1.22	0.006	−13	7	10	470
STD	0.065	0.061	0.151	1.25	1.58	0.04	35	35	129	138

Notice that the rotorcraft flies freely in a three-dimensional space without using any flying stand.

To explore the performance of the proposed controller, two sets experiments were performed. First, the quadrotor was tasked to hover at a desired altitude of 0.4 m when stabilizing all the angles and horizontal displacements at zero, starting from some initial configurations. Figures 7 and 8 show that the objective is achieved with very satisfying performance (see Table 3).

In the second experiment, we considered an autonomous flight. The aerial robot was tasked to take off, hover at a desired altitude for a predetermined period, and then land (see Fig. 9 and Table 3). The control law presented in the previous sections is shown to be robust with respect to parameter uncertainty and external disturbances by applying external forces to the aircraft during the period 225–330 s. From Figs. 9 and 10, we notice that the controller rejects these perturbations and the closed-loop system remains stable. In other experiments, we also applied disturbances on yaw and altitude, and the controller rejected them.

For quantitative analysis of the obtained results, we provided statistical descriptors (max, min, mean, and standard deviation STD) of the position, attitude, and input signals. Table 3 shows that the stabilization task is achieved with high accuracy. In the presence of external perturbations, the rotorcraft is not exactly stabilized at the expected position, but it still succeeds to maintain its position in a sphere of about 0.2 m of radius around the desired position (see Table 4 and Fig. 9). We believe that the small errors observed in Figs. 7–10 are mainly due to unmodeled dynamics, parameter uncertainty, and sensor noise.

VII. Conclusions

An efficient nonlinear control strategy for the quadrotor aircraft was proposed. The proposed control law is based on the nested-saturation technique and takes into account the boundedness of control inputs with improvements of the convergence speed of the closed-loop system. By using Lyapunov analysis, the convergence property was established for the complete model of the quadrotor helicopter, considering the coupling terms. In spite of the complexity of the convergence analysis, the control law is simple and performs satisfactorily in practice.

In this paper, we also described the embedded control system that was tested in real-time experiments. The results presented in this paper have shown the effectiveness and the good performance of our embedded control system. Indeed, experimental results have shown that the proposed control system is able to autonomously perform the tasks of taking off, hovering, and landing, even in the presence of external disturbances; this constitutes an important step forward in autonomous control of small rotorcraft.

Acknowledgments

This work was supported by the Picardie Region Council. We also acknowledge the anonymous reviewers for their valuable comments.

References

[1] Castillo, P., Lozano, R., and Dzul, A., *Modelling and Control of Mini-Flying Machines*, Springer–Verlag, New York, 2005.

[2] Shim, H., Koo, T. J., Hoffman, F., and Sastry, S., "A Comprehensive Study of Control Design of an Autonomous Helicopter," *Proceedings of the 37th IEEE Conference on Decision and Control*, Inst. of Electrical and Electronics Engineers, Piscataway, NJ, 1998, pp. 3653–3658.

[3] Vilchis, J. A., Brogliato, B., Dzul, A., and Lozano, R., "Nonlinear Modelling and Control of Helicopters," *Automatica*, Vol. 39, No. 9, Sept. 2003, pp. 1583–1596.

[4] Castillo, P., Dzul, A., and Lozano, R., "Real-Time Stabilization and Tracking of a Four Rotor Mini-Rotorcraft," *IEEE Transactions on Control Systems Technology*, Vol. 12, No. 4, July 2004, pp. 510–516.

[5] Kendoul, F., Fantoni, I., and Lozano, R., "Modeling and Control of a Small Autonomous Aircraft Having Two Tilting Rotors," *IEEE Transactions on Robotics and Automation*, Vol. 22, No. 6, Dec. 2006, pp. 1297–1302.

[6] "Unmanned Aerial Vehicles Roadmap 2000–2025," Office of the Secretary of Defense, Rept. AD-a391 358, Washington, D.C., 2001.

[7] Ollero, A., and Merino, L., "Control and Perception Techniques for Aerial Robotics," *Annual Reviews in Control*, Vol. 28, 2004, pp. 167–178.

[8] Frazzoli, E., Dahleh, M. A., and Feron, E., "Real-Time Motion Planning for Agile Autonomous Vehicles," *Journal of Guidance, Control, and Dynamics*, Vol. 25, No. 1, 2002, pp. 116–129.

[9] Gavrilets, V., Mettler, B., and Feron, E., "Control Logic for Automated Aerobatic Flight of Miniature Helicopter," AIAA Guidance, Navigation and Control Conference, Monterey, CA, AIAA Paper 2002-4834, 2002.

[10] Koo, T., and Sastry, S., "Output Tracking Control Design of a Helicopter Model Based on Approximate Linearization," *Proceedings of the 37th IEEE Conference on Decision and Control*, Inst. of Electrical and Electronics Engineers, Piscataway, NJ, 1998, pp. 3635–3640.

[11] Nieuwstadt, M. V., and Murray, R., "Rapid Hover to Forward Flight Transitions for a Thrust Vectored Aircraft," *Journal of Guidance, Control, and Dynamics*, Vol. 21, No. 1, Feb. 1998, pp. 93–100.

[12] Hauser, J., Sastry, S., and Meyer, G., "Nonlinear Control Design for Slightly Nonminimum Phase Systems: Application to V/STOL Aircraft," *Automatica*, Vol. 28, No. 4, 1992, pp. 665–679.

[13] Mahony, R., and Hamel, T., "Robust Trajectory Tracking for a Scale Model Autonomous Helicopter," *International Journal of Robust and Nonlinear Control*, Vol. 14, No. 12, Aug. 2004, pp. 1035–1059.

[14] Johnson, E. N., and Kannan, S. K., "Adaptive Trajectory Control for Autonomous Helicopters," *Journal of Guidance, Control, and Dynamics*, Vol. 28, No. 3, May–June 2005, pp. 524–538.

[15] La Civita, M., Papageorgiou, G., Messner, W. C., and Kanade, T., "Design and Flight Testing of an H_∞ Controller for a Robotic Helicopter," *Journal of Guidance, Control, and Dynamics*, Vol. 29, No. 2, Apr. 2006, pp. 485–494.

[16] Gavrilets, V., Mettler, B., and Feron, E., "Nonlinear Model for a Small-Sized Acrobatic Helicopter," AIAA Guidance, Navigation and Control Conference, Quebec, Canada, AIAA Paper 2001-4333, 2001.

[17] La Civita, M., Papageorgiou, G., Messner, W. C., and Kanade, T., "Design and Flight Testing of a Gain-Scheduled H_∞ Loop Shaping Controller for Wide-Envelope Flight of a Robotic Helicopter," *Proceedings of the 2003 American Control Conference*, Vol. 5, American Automatic Control Council, Evanston, IL, 2003, pp. 4195–4200.

[18] Leitner, J., Calise, A. J., and Prasad, J., "Analysis of Adaptive Neural Networks for Helicopter Flight Controls," *Journal of Guidance, Control, and Dynamics*, Vol. 20, No. 5, Oct. 1997, pp. 972–979.

[19] Kim, N., Calise, A. J., Hovakimyan, N., Prasad, J., and Corban, J. E., "Adaptive Output Feedback for High-Bandwidth Flight Control," *Journal of Guidance, Control, and Dynamics*, Vol. 25, No. 6, 2002, pp. 993–1002.

[20] Calise, A. J., Lee, S., and Sharma, M., "Development of a Reconfigurable Flight Control Law for Tailless Aircraft," *Journal of Guidance, Control, and Dynamics*, Vol. 24, No. 5, 2001, pp. 896–902.

[21] Johnson, E. N., and Calise, A. J., "Limited Authority Adaptive Flight Control for Reusable Launch Vehicles," *Journal of Guidance, Control, and Dynamics*, Vol. 26, No. 6, Dec. 2003, pp. 906–913.

[22] Wie, B., and Bernstein, D. S., "Benchmark Problems for Robust Control Design," *Journal of Guidance, Control, and Dynamics*,

Vol. 15, No. 5, Oct. 1992, pp. 1057–1059.
[23] Dornheim, M. A., "Report Pinpoints Factors Leading to YF-22 Crash," *Aviation Week and Space Technology*, McGraw–Hill, New York, Nov. 1992, pp. 53–54.
[24] Lauvdal, T., and Murray, R. M., "Stabilization of a Pitch Axis Flight Control Experiment with Input Rate Saturation," AIAA Conference on Guidance, Navigation, and Control, New Orleans, LA, AIAA Paper 1997-3638, 1997.
[25] Lauvdal, T., Murray, R. M., and Fossen, T. I., "Stabilization of Integrator Chains in the Presence of Magnitude and Rate Saturations: A Gain Scheduling Approach," *Proceedings of the 36th IEEE Conference on Decision and Control*, Vol. 4, Inst. of Electrical and Electronics Engineers, Piscataway, NJ, 1997, pp. 4004–4005.
[26] Murray, R. M., "Geometric Approaches to Control in the Presence of Magnitude and Rate Saturations," California Inst. of Technology, Rept. 99-001, 1999.
[27] Sussmann, J. H., Sontag, D. E., and Yang, Y., "A General Result on the Stabilization of Linear Systems Using Bounded Controls," *IEEE Transactions on Automatic Control*, Vol. 39, No. 12, Dec. 1994, pp. 2411–2425.
[28] Sussmann, J. H., and Yang, Y., "On the Stabilizability of Multiple Integrators by Means of Bounded Feedback Controls," *Proceedings of the 30th IEEE Conference on Decision and Control*, Inst. of Electrical and Electronics Engineers, Piscataway, NJ, 1991, pp. 70–72.
[29] Teel, A. R., "Global Stabilisation and Restricted Tracking for Multiple Integrators with Bounded Controls," *Systems and Control Letters*, Vol. 18, No. 3, Mar. 1992, pp. 165–171.
[30] Teel, A. R., "A Non Linear Small Gain Theorem for the Analysis of Control Systems with Saturation," *IEEE Transactions on Automatic Control*, Vol. 41, No. 9, 1996, pp. 1256–1270.
[31] Arcak, M., Teel, A. R., and Kokotovic, P., "Robust Nonlinear Control of feedforward Systems with Unmodeled Dynamics," *Automatica*, Vol. 37, Dec. 2001, pp. 265–272.
[32] Lozano, R., Castillo, P., and Dzul, A., "Global Stabilization of the PVTOL: Real-Time Application to a Mini-Aircraft," *International Journal of Control*, Vol. 77, No. 8, May 2004, pp. 735–740.
[33] , *Helicopter Performance, Stability, and Control*, Krieger, Malabar, FL, 1995.
[34] Conlisk, A., "Modern Helicopter Rotor Aerodynamics," *Progress in Aerospace Sciences*, Vol. 37, No. 5, July 2001, pp. 419–476.
[35] Etkin, B., *Dynamics of Flight*, Wiley, New York, 1959.
[36] Fantoni, I., and Lozano, R., *Non-Linear Control for Underactuated Mechanical Systems*, Communications and Control Engineering Series, Springer–Verlag, New York, 2002.
[37] McCormick, B. W., *Aerodynamics Aeronautics and Flight Mechanics*, Wiley, New York, 1995.
[38] Johnson, E. N., and Kannan, S. K., "Nested Saturation with Guaranteed Real Poles," *Proceedings of the 2003 American Control Conference*, Vol. 1, American Automatic Control Council, Evanston, IL, June 2003, pp. 497–502.
[39] Zavala-Rio, A., Fantoni, I., and Lozano, R., "Global Stabilization of a PVTOL Aircraft with Bounded Inputs," *International Journal of Control*, Vol. 76, No. 18, Dec. 2003, pp. 1833–1844.